Monolithic Multiwavelength VCSEL Array Using Cavity Patterning

Antoine Pissis[ORCID], Stefano Tirelli, Lorenzo Bosco, Viktoriia Gorbenko, Martin Suess, Urs Siegenthaler, David Quandt, Donato Bonfrate, Pratyush Das Kanungo, and Evgeny Zibik

Abstract—We report on a novel approach to adjust the emission wavelength of VCSEL devices. By patterning the Fabry-Perot cavity, we can control the effective refractive index of the optical mode and thus adjust the resonant wavelength. We developed a fabrication process based on 2 steps epitaxy and a lithographic cavity patterning to define the emission wavelength at the emitter level. A multiwavelength VCSEL array with a 30 nm wavelength tuning range around 940 nm is demonstrated.

Index Terms—VCSEL, wavelength control, WDM, multiwavelength laser, MOVPE growth, overgrowth.

I. Introduction

VERTICAL Cavity Surface Emitting Lasers (VCSELs) have been successfully deployed for short reach data transmission. Commercial VCSELs demonstrate a modulation bandwidth up to 25 GHz [1] while maintaining a low fabrication cost. Development of online services continues to drive the demand for a faster communication network. Wavelength Division Multiplexing (WDM) proposes to multiply the communication bandwidth by transmitting information using several wavelengths in parallel via one fiber. An example of cost-effective realization of a WDM transceiver is the use of a monolithic multiple wavelength VCSEL array. Such VCSEL arrays have been realized so far with the implementation of a growth rate gradient [2], the replacement of the top Distributed Bragg Reflector (DBR) by either a movable top mirror or a high contrast grating with different geometries [3] or the introduction of a phase tuning layer in the VCSEL cavity [4], [5].

We propose a technique based on patterning the cavity of the VCSEL to control the emission wavelength. We present the principle of this novel concept as well as the fabrication method and experimental results. The presented technique enables the monolithic fabrication of VCSELs with any emission wavelength within a range set by the difference of the optical lengths of etched and unetched cavities, and varying
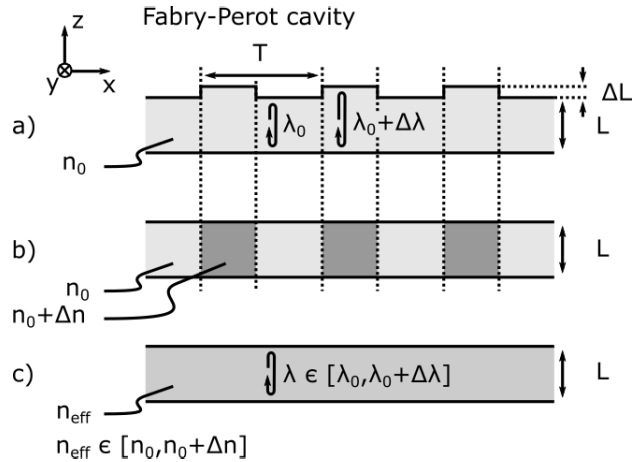
Fig. 1. Cross section of a patterned Fabry-Perot cavity a) with a periodic variation T of the cavity thickness, b) with a variation of local refractive index, and c) with an uniform effective refractive index and thickness.

according to their lithographic cavity patterning. In this work, we demonstrated a 30 nm-wide tuning range of wavelengths centered around 940 nm.

II. Cavity Patterning for Wavelength Engineering

We employed a model based on the effective refractive index approximation to verify how patterning a Fabry-Perot cavity allows to adjust its resonant wavelength in a VCSEL.

A Fabry-Perot resonator is typically formed by two reflectors facing one another separated by a layer with refractive index n_0 and thickness L both uniform in the plane of the reflector. In such resonator, the wavelength in the air λ_0 of the supported standing waves must satisfy the following formula:

$$n_0 L = \frac{m}{2} \lambda_0 \tag{1}$$

where m is an integer.

Let us consider a Fabry-Perot cavity where the distance separating the two reflectors alternates between two thicknesses L and $L + \Delta L$ over the plane of the reflector (xy plane). While the thickness variation could follow any profile, we consider, for simplicity, that the top reflector profile is a grating with period T as presented in Fig. 1a. If the grating period is large compared to the resonant wavelength, we can assume that the regions of thickness L and $L + \Delta L$ behave as independent Fabry-Perot resonators supporting the wavelengths λ_0 and

$\lambda_0 + \Delta\lambda$. However, when the grating period is comparable to the resonant wavelength, the optical mode overlaps the regions with different cavity thicknesses. In this case, the regions with the different thicknesses form a unique Fabry-Perot cavity. To understand the optical mode formation in this patterned cavity, we turn the variation of cavity thickness ΔL into an equivalent variation of refractive index Δn as shown in Fig. 1b. To link their values, we use the model proposed by Hadley [6] which, applied to our problem, is formulated by:

$$\frac{\Delta n}{n_0} = \frac{\Delta\lambda}{\lambda_0} \qquad (2)$$

Now that the information of cavity thickness alteration is embedded in the plane of the mirror and expressed in terms of variation of refractive index, we can compute the supported transverse mode propagating orthogonally to the plane of the mirror (z direction) using standard 2D electromagnetic waveguide simulation. We simulated the periodic configuration with 1D and 2D gratings with various fill factors. We used COMSOL EM module and simulated the unit cell by applying Floquet periodic boundary conditions [7]. The unit cell is formed by an inner region of refractive index $n_0 + \Delta n$, corresponding to the cavity region of thickness $L + \Delta L$, surrounded by a region of refractive index n_0, corresponding to the cavity region of thickness L. To match our experimental results, we used the refractive index $n_0 = 3.55$ and refractive index ratio $\Delta n/n_0 = 2\%$. These values were extracted from the experimental data, by comparing the resonance wavelength of VCSELs whose the cavity tuning layer is fully etched and unetched. Fig. 2a and Fig. 2b show electric field intensity profile of the first order transverse mode for a 1D linear grating and a 2D square grating. As expected, the high intensity regions of the optical field are concentrated in the high index regions. Fig. 2c and Fig. 2d exhibit measured near field of actual VCSELs with cavity pattern of the same respective geometry for comparison. The experimental results also show the confinement of the optical mode by the circular oxide aperture. It is worth noting the influence of the cavity pattern on the distribution of the optical mode. This confirms that a modification of the local longitudinal resonance has a significant impact on the transverse optical mode distribution. The fabrication method we used is detailed in the next section.

Finally, despite the intensity of the optical mode being modulated by the geometrical grating pattern inside the cavity, the optical mode also overlaps with the regions where the refractive index is lower. Hence, we can use the effective refractive index approximation, which contains the information of the refractive index distribution of the pattern. In this case, the patterned cavity can be represented as a conventional Fabry-Perot cavity with a uniform effective refractive index n_{eff} and uniform thickness L as depicted in Fig. 1c. Then relation 1 can be rewritten as:

$$n_{eff}L = \frac{m}{2}\lambda_0 \qquad (3)$$

where m is an integer.

This relation implies that altering the transverse mode effective refractive index, which is done here by cavity patterning,
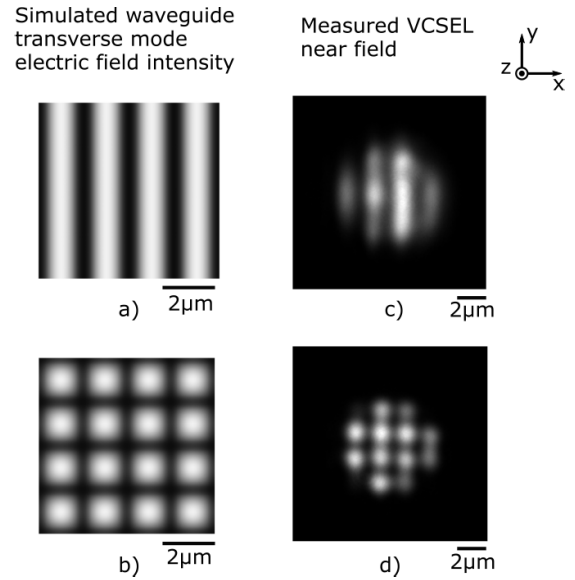

Fig. 2. Comparison of simulated (a,b) and measured (c,d) near fields of VCSEL with patterned cavity.

modifies the resonant wavelength of the cavity. In the following parts, we show how we used this principle to fabricate multiwavelength VCSEL array.

III. METHOD AND FABRICATION

The emission wavelength in a VCSEL is defined by a Fabry-Perot cavity. Modern MOVPE (Metalorganic Vapor Phase Epitaxy) and MBE (Molecular Beam Epitaxy) systems are optimised to deliver uniform layers with deviations of less than 1% across 6-inch diameter wafer. It is possible to grow nonuniform cavity thickness in a controlled manner, e.g., by patterning the substrate [8] or by varying the growth temperature on the surface [9]. However, the disadvantage of these methods is that it is challenging to control the thickness on short distances, thus limiting their applicability. According to our model, we can adjust the emission wavelength of a VCSEL by patterning the cavity. However, this cannot be achieved within a single epitaxial growth. For this reason, we accomplished a patterned cavity by dividing the growth of the VCSEL epitaxial structure into two sub-growths and introducing a grating in the cavity [10].

We start with growing an AlGaAs bottom Distributed Bragg Reflector (DBR) on a GaAs substrate followed by the first section of the cavity containing the active region formed by InGaAs quantum wells (QWs) and terminating with a GaAs layer. Then, we define and etch grating patterns in the last GaAs layer at the location of the future emitters using an optical lithography process. The grating depth is chosen considering the unpatterned cavity thickness and the desired wavelength range $\Delta\lambda$. The wavelength range corresponds to the wavelength shift between the etched and non-etched cavity regions. In our demonstration, the ratio between wavelength range and wavelength in unpatterned cavity $\Delta\lambda/\lambda_0$ does not exceed few percent. The different geometries with varying fill factor, associated to the desired wavelengths, are defined in a single photolithography step. The wafer goes back to
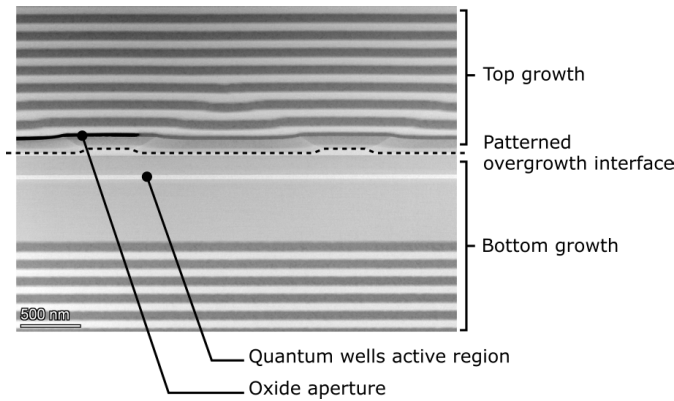
Fig. 3. TEM image of a patterned VCSEL cavity with oxidized aperture.

Fig. 4. Measured spectra from different VCSEL emitters with 1 μm-periodic linear grating and increasing fill factor from left to right.

Fig. 5. Simulated effective refractive index for linear grating of different periods and measured wavelength at maximal intensity according to the grating fill factor with a grating period of 1 μm and 2 μm.

the growth reactor where the remaining part of the cavity and the top DBR are grown. The aluminum-free layer at the overgrowth interface guarantees a high-quality overgrowth with a low defect density. A high-aluminum concentration AlGaAs layer in the first mirror pair is used to form the oxide aperture via the oxidation process.

Fig. 3 presents a TEM image showing the cross-section view of our VCSEL patterned cavity. Between the active region and the oxide aperture, we observe the overgrowth interface following the pattern profile defined during etching. It is also depicted by a dotted line for clarity. It can be seen that the pattern propagates within the first several mirror pairs before it gets completely planarized. Despite the high Al content AlGaAs layer being non-planar, we were able to controllably oxidize the structure and form the oxide aperture for current and optical mode confinement.

The overgrowth together with the lithographic process enables VCSELs with a patterned cavity. In addition to being compatible with the standard oxidation process for AlGaAs based VCSELs, this technique allows us to define the wavelength for a specific emitter. Thus, this method presents the flexibility to set a wavelength shift between neighboring emitters processed on the same substrate by etching a grating with different fill factors within one etching step. This enables the design of customizable multiwavelength VCSEL array.

IV. RESULTS AND DISCUSSION

To demonstrate the feasibility of multiwavelength VCSEL arrays, we fabricated 6 μm oxide aperture VCSEL emitters on a 3-inch diameter wafer with patterned cavity. We investigated multiple pattern geometries from one emitter to the other with an emitter pitch of 200 μm on the same substrate.

Fig. 4 shows an optical image of an area of the wafer where we examined VCSEL cavities patterned with linear gratings of period 1 μm with fill factor ranging from 0 to 1 over 11 emitters. The emitters are uncoupled and have their own metal contact, so each associated cavity pattern is characterized individually. The spectra of each emitter measured at 5 mA operating current at room temperature are reported in Fig. 4. The multiple peaks forming each spectrum indicate that the devices are operating in the multi-mode regime. However, the spectra from the different emitters cover a 30 nm-wide wavelength range around 940 nm. As our model predicted, the
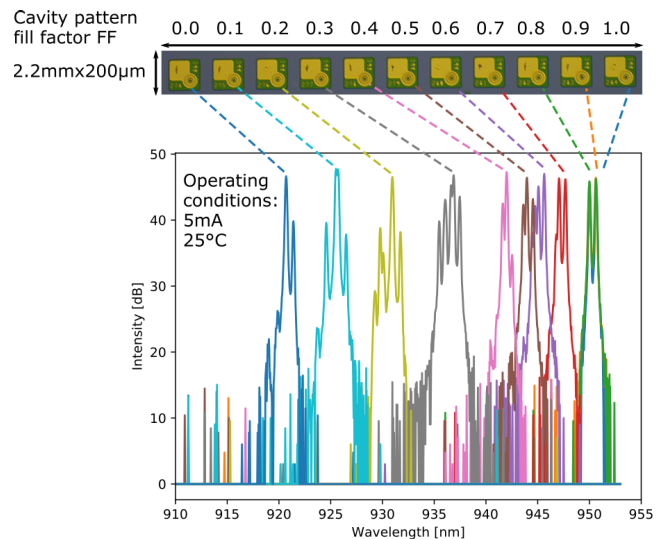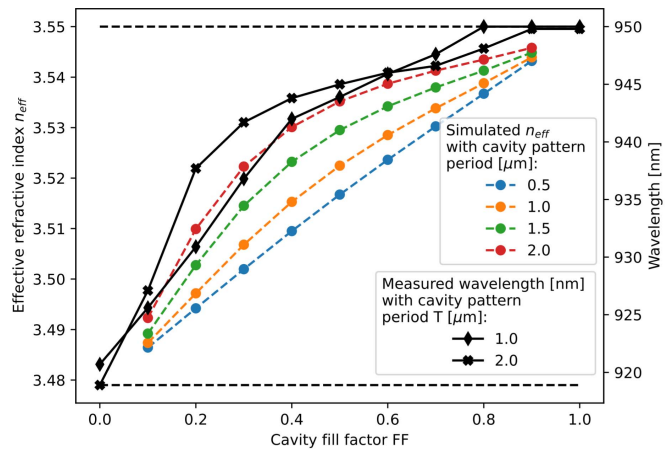
peak wavelength, estimated at the maximal intensity, depends on the local geometry of the cavity pattern. In this case, we observe that the emission wavelength increases together with the fill factor of the grating.

To further compare these experimental results to our model, we report on Fig. 5 the dependence of the simulated effective refractive index of the cavity zero order transverse mode, obtained for linear grating of period from 2 μm down to 0.5 μm, versus linear the grating fill factor. Relation 3 shows a linear dependence between the effective refractive index and the resonant wavelength; therefore, we can overlay the measured peak wavelengths from Fig. 4 with the simulated refractive indexes. We obtained an overall good matching between the evolution of the simulated refractive index and the measured peak wavelength. The discrepancy can be attributed to the fact that the real fill factor differs from the nominal one, due to optical lithography limitations. However, the model confirms and explains the nonlinear relation between the grating fill factor and the measured wavelength. The model
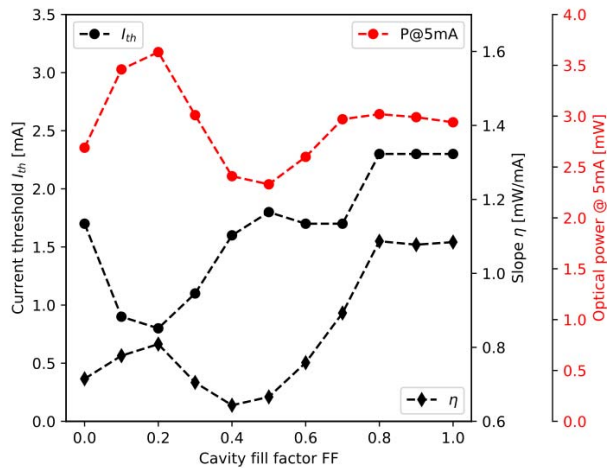
Fig. 6. Threshold current, slope efficiency and optical power measured at 5 mA versus the grating fill factor.

also shows that the linear dependence between the emission wavelength on the grating fill factor can be improved by bringing down the grating period close to the wavelength dimension. We confirmed experimentally that a 1 µm grating period gives an enhanced wavelength control compared to a 2 µm grating period. While we observed an abrupt wavelength variation between 935 nm and 925 nm with a 2 µm grating period, we were able to reach wavelengths in this same range with a 1 µm grating period.

In terms of electro-optical performance, Fig. 6 shows the variation of optical power of the multiwavelength VCSEL array presented in Fig. 4 by driving the emitters individually at 5 mA. While the produced optical power is not constant across the array, the power variation remains below 2 dB. This variation of optical power arises from the variations of threshold current I_{th} and slope efficiency η between emitters also represented in Fig. 6. The variations of threshold current and slope efficiency are also observed in the cavity phase tuning layer approach as studied in [11]. We attribute the variation of electro-optical performance to the dependence of the active region gain and DBR reflectivity with the operating wavelength. Other effects like the variation of the optical confinement factor and the introduction of scattering losses generated by the patterned features in the cavity can also impact the electro-optical performance.

V. CONCLUSION

We proposed and demonstrated a novel method to adjust the emission wavelength of a VCSEL by patterning the cavity to control the effective refractive index of the lasing mode. Splitting the growth of the VCSEL cavity in two steps to introduce a pattern enables the definition of a wavelength offset between any emitter within the wafer. This method is compatible with the oxide aperture VCSEL technology. We successfully fabricated an addressable VCSEL array delivering a wavelength control over a 30 nm-wide range around 940 nm. This technique is not exclusive to a specific material system; thus, wavelength control over other wavelength domains can be investigated as well using the same principle.

REFERENCES

[1] IIVI. *25G VCSEL Array—Dual Top Contact.* Accessed: Jun. 24, 2021. [Online]. Available: https://ii-vi.com/product/25g-vcsel-array-dual-top-contact

[2] C. J. Chang-Hasnain, "Tunable VCSEL," *IEEE J. Sel. Topics Quantum Electron.*, vol. 6, no. 6, pp. 978–987, Nov./Dec. 2000.

[3] V. Karagodsky, B. Pesala, C. Chase, W. Hofmann, F. Koyama, and C. J. Chang-Hasnain, "Monolithically integrated multi-wavelength VCSEL arrays using high-contrast gratings," *Opt. Exp.*, vol. 18, no. 2, pp. 694–699, 2010.

[4] Y. Kawakita, K. Takaki, M. Funabashi, S. Imai, and A. Kasukawa, "1060 nm single-mode multi-wavelength VCSEL array with intra-cavity phase tuning layers," in *Proc. Int. Semiconductor Laser Conf.*, Sep. 2014, pp. 207–208.

[5] M. Jahed, J. S. Gustavsson, and A. Larsson, "Precise setting of micro-cavity resonance wavelength by dry etching," *J. Vac. Sci. Technol. B*, vol. 37, no. 3, May 2019, Art. no. 031217.

[6] G. R. Hadley, "Effective index model for vertical-cavity surface-emitting lasers," *Opt. Lett.*, vol. 20, no. 13, pp. 1483–1485, Jul. 1995. [Online]. Available: http://ol.osa.org/abstract.cfm?URI=ol-20-13-1483

[7] Olin. (2022). *Modeling Periodic Structures in COMSOL Multiphysics.* COMSOL. [Online]. Available: https://www.comsol.com/video/modeling-periodic-structures-in-comsol-multiphysics

[8] F. Koyama, T. Mukaihara, Y. Hayashi, N. Hatori, K. Iga, and N. Ohnoki, "Two-dimensional multiwavelength surface emitting laser arrays fabricated by nonplanar MOCVD," *Electron. Lett.*, vol. 30, no. 23, pp. 1947–1948, Nov. 1994.

[9] D. E. Bossi, W. D. Goodhue, M. C. Finn, K. Rauschenbach, J. W. Bales, and R. H. Rediker, "Reduced-confinement antennas for GaAlAs integrated optical waveguides," *Appl. Phys. Lett.*, vol. 56, no. 5, pp. 420–422, Jan. 1990.

[10] *Patent Has Been Filed by II-VI Incorporated*, Saxonburg, PA, USA, Nov. 2020.

[11] M. Jahed, J. S. Gustavsson, and A. Larsson, "VCSEL wavelength setting by intra-cavity phase tuning—Numerical analysis and experimental verification," *IEEE J. Quantum Electron.*, vol. 57, no. 6, pp. 1–7, Dec. 2021.